coatings

MDPI

Communication

Annealing Effect on Microstructure of Novel Ti Doped DLC Multilayer Films

Shidong Zhang [1], Guang Jiang [1], Yang Yang [2], Hongtao Li [3], Fuyao Yan [1], Mufu Yan [1,*] and Yanxiang Zhang [1,*]

[1] National Key Laboratory for Precision Hot Processing of Metals, School of Materials Science and Engineering, Harbin Institute of Technology, Harbin 150001, China; stone_hit@163.com (S.Z.)
[2] Key Laboratory of Green Fabrication and Surface Technology of Advanced Metal Materials, Research Center of Modern Surface and Interface Engineering, Anhui University of Technology, Maanshan 243002, China
[3] College of Materials Science and Engineering, Nanjing Tech University, Nanjing 210009, China
* Correspondence: yanmufu@hit.edu.cn (M.Y.); hitzhang@hit.edu.cn (Y.Z.)

Abstract: Diamond-like films (DLC) are an exceptional engineering material with excellent performance such as high hardness, low friction coefficient, superior wear resistance and chemical inertness. However, two major problems of high internal stress and poor thermal stability have seriously limited its industrial applications. In particular, the microstructures and properties of pure DLC films are highly sensitive to high temperature. Therefore, the purpose of this study is to investigate the effect of annealing temperature on the microstructures of the as-prepared films. Ti-doped DLC multilayer films were synthesized by closed field unbalanced magnetron sputtering. The as-deposited films were annealed in the range of 200 to 800 °C. The surface morphology, phase structure and bonding structure of the films were characterized by SEM, AFM, GIXRD and Raman spectroscopy. The resulting films remained a smooth surface after annealing and maintained the nature of amorphous carbon up to 600 °C. The formed phases of graphite carbon and TiC nanocrystallines occur above 600 °C. In addition, the D- and G-bands showed a significant blue shift and the $FWHM_G$ shows a declining trend up to 600 °C. This result revealed that the films had high graphitization temperature and good thermal stability due to the formation of TiC nanocrystallines and its novel structure design containing elemental doping, multilayer structuring and functionally graded layering.

Keywords: magnetron sputtering; diamond-like films; microstructures; thermal stability

Citation: Zhang, S.; Jiang, G.; Yang, Y.; Li, H.; Yan, F.; Yan, M.; Zhang, Y. Annealing Effect on Microstructure of Novel Ti Doped DLC Multilayer Films. *Coatings* **2023**, *13*, 833. https://doi.org/10.3390/coatings13050833

Academic Editors: Ben Beake and Jose Luis Viesca

Received: 26 March 2023
Revised: 15 April 2023
Accepted: 21 April 2023
Published: 26 April 2023

1. Introduction

In the past half century, diamond-like carbon (DLC) films have aroused widespread attention due to a wide range of extraordinary performance of high hardness, low friction coefficient, low dielectric constant, wide band gap, good optical transparency and biocompatibility, superior wear resistance and chemical inertness [1–4]. Hence, it has been widely applied in aerospace, mechanical, electrical, biomedical, optical, tribological and automotive fields [5–10]. Since Aisenberg and Chabot were the first who successfully deposit DLC films at room-temperature substrates using an ion beam deposition technique in 1971 [11], researchers have been devoting their efforts to the synthesis of DLC films using various deposition techniques, including plasma-enhanced chemical vapor deposition (PECVD), microwave plasma CVD (MPCVD), electron assisted CVD (EACVD), pulse laser deposition (PLD), filtered cathodic vacuum arc (FCVA), ion beam deposition (IBD) and magnetron sputtering (MS) [12–17]. In this work, MS has been adopted due to many advantages, such as low deposition temperature, high deposition efficiency, large area deposition, low impurity level and good bonding strength [18]. However, two major drawbacks of DLC films with high internal stress [19,20] and poor thermal stability [21,22] have severely restricted its industrial applications under harsh service conditions such as high temperature and severe chemical corrosion. The internal stress is in a wide range from a few GPa to 10 GPa [23], which result in poor adhesion strength and low film thickness.

In general, the pure DLC films occurred via graphitization from sp^3 to sp^2 hybridized bonds beyond 200 °C [24,25] and severe oxidation existed above 300~400 °C, leading to a sharp deterioration in film performance [26,27]. To solve these problems, researchers have developed many effective approaches such as elemental doping, multilayer structuring, functionally graded layering and thermal annealing [28,29]. As reported in our previous work [5], the as-prepared novel Ti-doped DLC multilayer films have utilized the above mentioned methods of elemental doping, multilayer structuring and functionally graded layering. The thus-prepared DLC films had good adhesion strength and also obtained excellent mechanical, tribological and anti-corrosive properties by magnetron sputtering. Here, we mainly focus on thermal stability of these novel DLC films. Specifically, the effect of annealing temperatures on the microstructure was investigated using Raman Spectroscopy. In addition, there are relatively few reports on the high-temperature (800 °C) thermal stability of Ti-doped DLC multilayer films.

2. Materials and Methods

2.1. Film Preparation and Annealing Treatment

The as-deposited films were deposited onto 17-4PH polished surfaces and Si (100) wafers by closed field unbalance magnetron sputtering. In this sputtering system, one graphite target and one titanium target (99.99%) were utilized. The dimensions of these two targets were 300 mm × 100 mm × 8 mm. The diameter of the vacuum chamber was 200 mm and ion current density was larger than 30 mA/cm^2. In order to obtain better film uniformity, the substrate and sample holder can realize rotation and revolution (4.5 rpm), respectively. Prior to the deposition, these polished surfaces needed ultrasonic cleaning using acetone, ethanol and deionized water, respectively, for more than 5 min. The base pressure was kept at 4.0×10^{-3} Pa using mechanical pump and molecular pump. Then, high purity argon gas (99.99%) with a flow rate of 16 mL/min was introduced to maintain at about 0.5 Pa for deposition pressure. The deposition temperature was lower than 200 °C. Table 1 describes five steps of the film deposition, including argon ion cleaning, deposition of the Ti layer, gradient layer, composite layer and DLC layer. The composition of the corresponding layers was controlled by modulating the respective target current, which is vital to the microstructure and property of the films, especially for the Ti doping level. In this study, designed titanium target currents of composite layer and DLC layer are 0.4 A and 0.1 A, respectively. The detailed deposition process was described in our previous work [5]. Thermal annealing treatment was performed at 200, 400, 500, 600 and 800 °C in a quartz tube furnace (Type SX2-8-10, XinNuo company, Shanghai, China) at 1×10^{-2} Pa for 1 h.

Table 1. The deposition process of the as-deposited films.

STEP	Ti Target Current (A)	C Target Current (A)	Substrate Bias Voltage (−V)	Time (min)
Ion cleaning	0.3	0	400	30
Ti layer	5.5	0	70	30
Gradient layer	5.5 → 0.4 [a]	0 → 1.5 [a]	70–65 [b]	60
Composite layer	0.4	1.5	65	120
DLC layer	0.1	1.5	65	240

[a] The currents of Ti and C Target were linearly changed in 60 mins. [b] The Substrate Bias Voltage was changed from 70 to 65 (−V).

2.2. Characterization of the As-Deposited Films

The surface morphology of the as-prepared films was characterized by scanning electron microscope (SEM, type SUPRA55, Zeiss, Jena, Germany). The elemental composition of the film surface was examined by energy dispersive spectrometer (EDS, Zeiss, Jena, Germany). The three-dimensional morphology and roughness of the film surface were measured in tapping mode over 3 μm × 3 μm by an atomic force microscope (AFM, type

Dimension Fast scan, Bruker, Billerica, MA, USA). The chemical bonds of the films were measured by Raman spectroscopy (Renishaw inVia, Chatswood, Australia). The excitation wavelength was 532 nm from a diode-pumped solid-state laser. The phase structure of the films was identified by grazing incidence X ray diffraction (GIXRD, type Philips X' Pert) in the continuous scanning mode with Cu-Ka radiation (λ = 0.15406 nm) at 40 kV and 40 mA. The θ–2θ scanning configuration was in the range of 10–90°. Step size and grazing incidence angle were 0.02° and 1°, respectively.

3. Results

3.1. Surface Morphology and Chemical Composition of the As-Deposited Films

Figure 1 illustrates that surface morphologies of the as-deposited films annealed at different temperatures from 200 to 800 °C. As temperature increases, the internal stress of the hydrogen-free DLC films is gradually released, and microcracks and delamination are often generated [30]. However, Figure 1 shows that all the as-prepared film surfaces have no defects and remain the nature of amorphous carbon, which mainly benefits from the novel design of Ti-doped multilayer gradient structure. Comparing to the untreated film surface in our previous work [5], there is no significant change in the treated film surfaces below 500 °C. These smooth surfaces have similar spherulitic characteristics which are composed of numerous stacked amorphous carbon clusters. As the temperature rises to 600 °C, the boundaries of amorphous carbon clusters begin to change slightly. Besides, a large amount of white dots appear on the film surface at 800 °C, indicating relatively severe oxidation. The surface chemical composition of the film surfaces corresponding to the selected areas is given in Table 2. It can be noted that the C and Ti content in the film is about 75 at % and 21 at %, respectively. The C content initially decreases from 200 to 600 °C and then increases with the temperature increases up to 800 °C, while the Ti content displays an opposite trend. Moreover, the O content is maintained at a lower content and its content increases with the temperature increases. The surface of the films annealed at 800 °C has the highest O content of 4.39 at %, which is in correspondence with the obvious changes in surface morphology shown in Figure 1e. The phase structures and characteristic peaks of amorphous carbon will be clarified by the following analysis of GIXRD and Raman spectra.

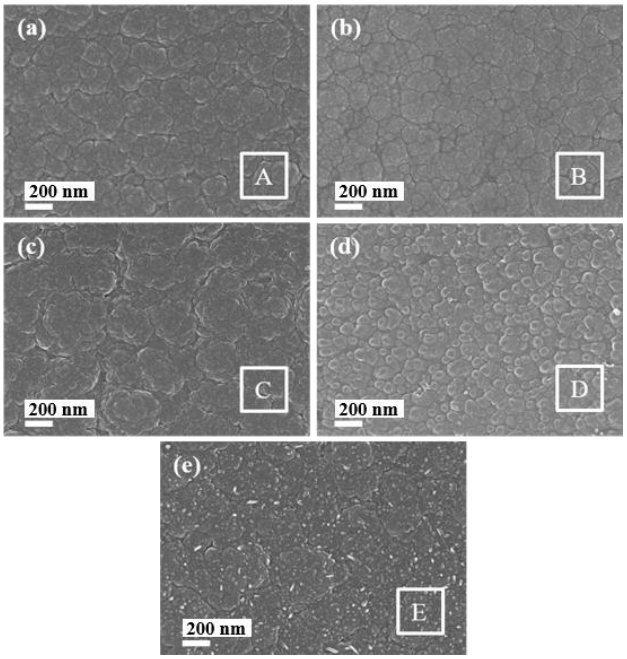

Figure 1. SEM surface morphologies of the as-deposited films annealed at different temperatures: (**a**) 200 °C, (**b**) 400 °C, (**c**) 500 °C, (**d**) 600 °C, (**e**) 800 °C.

Table 2. Surface chemical composition of the as-deposited films annealed at different temperatures corresponding to the selected areas in SEM images were determined from EDS.

Content	C (at %)	Ti (at %)	O (at %)
Region A	75.49	21.88	2.70
Region B	75.21	21.99	2.80
Region C	74.74	22.04	3.22
Region D	74.41	21.95	3.64
Region E	75.36	20.25	4.39

Figure 2 presents the typical three-dimensional morphologies of the films treated at the room temperature and different annealing temperatures from 200 to 800 °C. Compared with the untreated film surface, the surface morphologies of the annealed films have similar features with the relatively smoother cone-shaped protruding nanoclusters (gray structure in Figure 2) and the relatively rougher prolonged protrusions (white structure in Figure 2). Figure 3 shows the surface roughness of the as-deposited films annealed at various temperatures. In all cases, the roughness of the films remains below 12 nm and the roughness of the annealed films is lower than that of the untreated films. Moreover, both the root mean square roughness (R_q) and the average roughness (R_a) of the films treated at different temperatures have the same changing tendency. This result is contrary to the report of Osanai et al. [31]. Specifically, the roughness of the films first linearly decreases as the temperature rises to 500 °C and then increases with the temperature increasing up to 800 °C. This result is due to the formation of fine graphite grains accompanied by mild graphitization at the lower temperature, whereas it is ascribed to the formation of larger amount and size of nanocrystal graphite clusters and TiC nanocrystallines at the higher temperature [29]. The TiC nanophase is evident in the following XRD analysis.

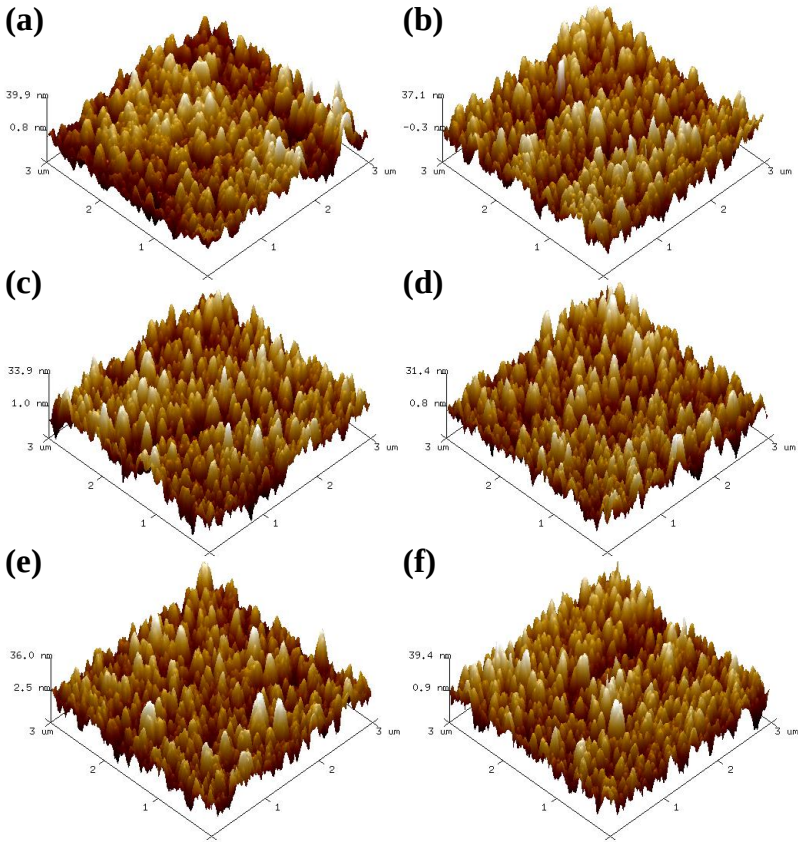

Figure 2. AFM three-dimensional morphologies of the as-deposited films annealed at different temperatures: (**a**) untreated, (**b**) 200 °C, (**c**) 400 °C, (**d**) 500 °C, (**e**) 600 °C, (**f**) 800 °C.

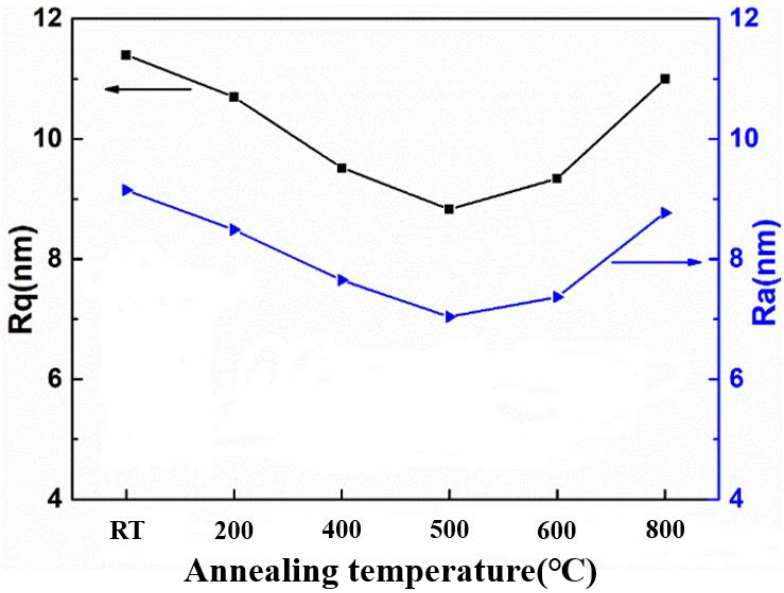

Figure 3. Surface roughness of the as-deposited films annealed at different temperatures.

3.2. Phase Analysis of the As-Deposited Films

Figure 4a shows the XRD spectra of the as-deposited films with different annealing temperatures. It can be seen that all these XRD patterns have phases of TiC, α-Ti and α-Fe, whereas the graphite carbon phase occurs when the temperature exceeds 600 °C, suggesting that amorphous carbon structure undergoes graphitization and crystallization at high temperature. This result indicates that the films still remain in its amorphous structure up to 600 °C, which is consistent with the above SEM result in Figure 1d. It also reveals that the graphitization temperature of the films is above 600 °C, which is mainly attributable to the above mentioned novel structures containing the formation of TiC nanocrystallines, which is consistent with the results of Martnez-Martnez et al. [32]. Three peaks at 36.0°, 41.8° and 60.6° can be well-indexed to (111), (200) and (220) crystal planes of TiC nanocrystalline (ICSD 89-3828), respectively. The formed TiC nanocrystallines are also verified by TEM analysis in our previous work [5]. In addition, the broad diffraction peaks of α-Ti phase and TiC nanocrystalline are attributed to the smaller size of phases with poor crystallinity embedded in the amorphous carbon films when the annealing temperature is below 400 °C; these broad diffraction peaks become sharper as the temperature increases to 800 °C, suggesting that it generates the larger amount and size of TiC nanocrystallines. Therefore, it is believed that the increasing annealing temperature is beneficial for the graphitization of amorphous carbon and the formation of TiC nanocrystalline.

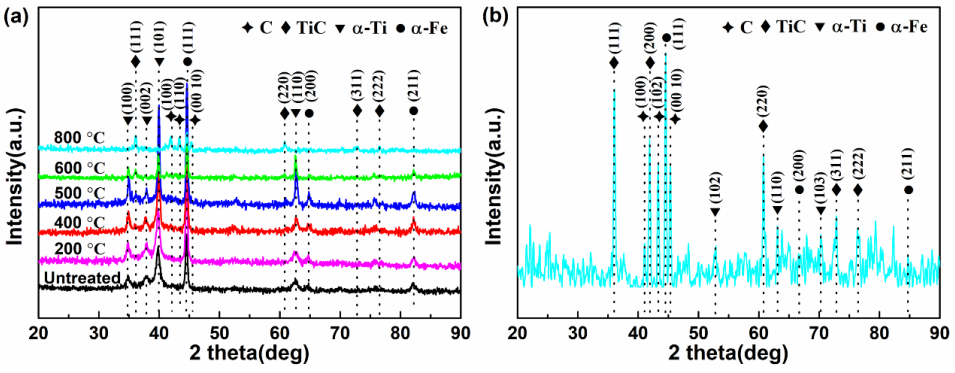

Figure 4. (**a**) XRD spectra of the as-deposited films annealed at different temperatures; (**b**) annealed at 800 °C.

3.3. Microstructure Analysis of the As-Deposited Films

In order to investigate the presence of amorphous carbon, Raman spectroscopy is used to analyze its bonding structures. Figure 5 illustrates the Raman spectra of the films annealed at different temperatures. These measured Raman spectra have similar features compared with the previous work [26,33]. The D- and G-bands are distinctly separated at 500 °C and the separation increases with increasing temperature. Moreover, the typical D- and G- bands of amorphous carbon are still observed below 800 °C. This result indicates that the as-grown films have high graphitization temperature and good thermal stability, which mainly benefits from the novel Ti-doped multilayer gradient structure.

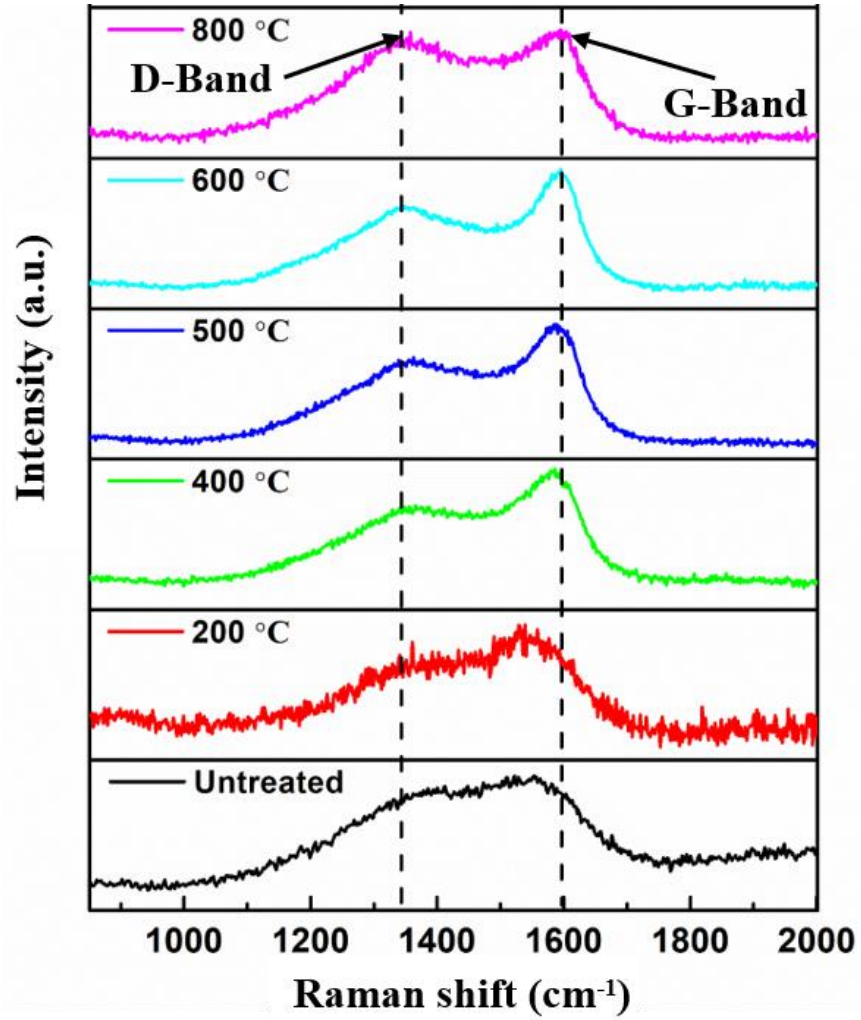

Figure 5. Raman spectra of the as-deposited films annealed at different temperatures.

Figure 6 shows that the Raman spectra of the films annealed at different temperatures exhibit a broad peak in 1000–1800 cm^{-1} region. So it can be deconvoluted into D-band ("disordered") and G-band ("graphitic") [4,34] using a Gaussian function. The D-band is located at approximately 1370 to 1400 cm^{-1}. The G-band is centered at 1580 ± 10 cm^{-1}. The D- and G-bands are attributed to sp^2 sites. The G-band is ascribed to the bond stretching E_{2g} modes of all pairs of sp^2 hybridized carbon atoms in both rings and chains. The D-band arises from the breathing A_{1g} modes of sp^2 atoms in rings [35–40]. The detailed deconvoluted parameters are given in Table 3.

Table 3. The results of deconvoluted Raman spectra in Gauss-Lorenz method.

Annealing Temperature (°C)	R_I I_D/I_G (%)	D Band Position/*FWHM* (cm^{-1})		G Band Position/*FWHM* (cm^{-1})	
untreated	132	1386	293	1569	153
200	95	1395	337	1584	101
400	101	1399	360	1584	98
500	95	1389	339	1588	92
600	83	1376	316	1589	89
800	118	1373	307	1590	112

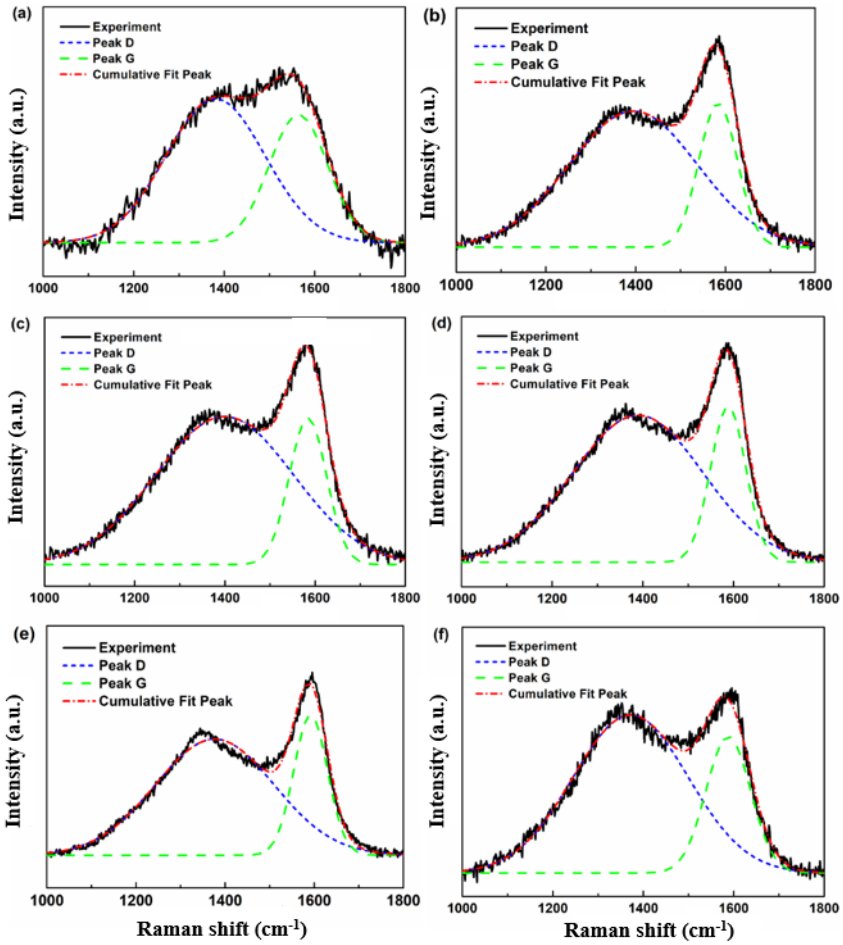

Figure 6. The deconvoluted Raman spectra of the as-deposited films annealed at different temperatures: (**a**) untreated, (**b**) 200 °C, (**c**) 400 °C, (**d**) 500 °C, (**e**) 600 °C, (**f**) 800 °C.

Figure 7 reveals the annealing effect on the structure of D- and G-bands. The integral intensity ratio of the D peak to the G peak (I_D/I_G ratio) is a measure of disorder of sp^2 C in the amorphous carbon films [40]. Figure 7a shows that the I_D/I_G ratio of the films after annealing is lower than that of untreated films, indicating the deceasing disorder of the treated films. In addition, there are three stages of the I_D/I_G variation tendency with the temperature increases. In the first stage at the lower temperature (200–400 °C), the I_D/I_G slightly increases with the temperature increases. In the second stage at the middle temperature (400–600 °C), the I_D/I_G shows an almost linear declining trend as temperature increases. In the last stage at the higher temperature (600–800 °C), the I_D/I_G exhibits a sharp increasing trend as the temperature increases. This result is different from the report of Orwa et al. [41], which is caused by the large uncertainties and complexities of structural changes of various amorphous carbon films during the annealing process. Figure 7a also

demonstrates that the position and intensity of D-band first increase and then decrease with the increase of temperature. Figure 7b plots the G peak position and the G peak full width at half maximum ($FWHM_G$) as a function of annealing temperature. Above 200 °C, the G-band position almost linearly increases as the temperature increases. The $FWHM_G$ of annealed films is lower than that of untreated films and the $FWHM_G$ linearly decreases with the increasing temperature up to 600 °C. These results are consistent with numerous reports [42–44]. As the temperature increases to 800 °C, the $FWHM_G$ abruptly rises to a higher value.

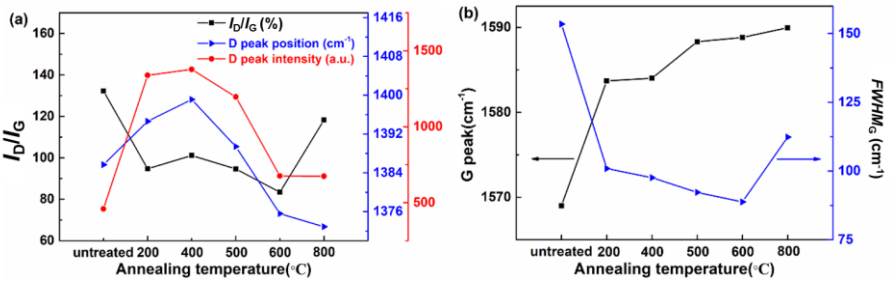

Figure 7. The annealing temperature evolved characters with various parameters from D- and G-bands (**a**) the I_D/I_G ratio, the position and intensity of D-band, (**b**) the position and full width at half maximum (*FWHM*) of G-band.

In general, the above phenomenon could be account for based on the following reasons. The amount and size of the formed nano-crystalline graphitic domains in the films are quite small below 200 °C. Thus, these small domains are weakly coupled with the laser beam of the Raman spectrum, leading to no significant change in the D- and G-bands in Figure 5. As the temperature increases from 200 to 600 °C, the D- and G-bands gradually separate and their symmetry increases, and the G-band shows a significant blue shift and the $FWHM_G$ shows a downward trend, indicating a tending toward similar Raman characteristics of microcrystalline graphite. It reveals that the bond angle disorder of sp^2 C decreases and the clusters growth of sp^2 C and nanocrystal graphite in the films. The phase of graphite carbon is observed by the above XRD results. The nanocrystal graphite clusters are possibly directly formed by the clustering of sp^2 C or generated by the clustering after the transition from sp^3 C to sp^2 C [33].

4. Conclusions

The novel Ti-doped DLC multilayer films were prepared using closed field unbalanced magnetron sputtering technique. The thermal stability of the as-prepared films annealed at different temperatures was investigated by SEM, AFM, XRD and Raman spectroscopy. The most important results were summarized as follows.

(1) The surface morphology of the as-deposited films has no significant change below 600 °C. The surface roughness of the films (<12 nm) decreased after annealing. The roughness of the annealed films initially decreased and then increased with the temperature increases;
(2) The formation of graphite carbon phase occurs and the diffraction peaks of TiC phase becomes more obvious above 600 °C. The films remained the nature of amorphous carbon structure up to 600 °C and oxidation occurred at 800 °C, indicating its high graphitization temperature and good thermal stability;
(3) The D- and G-bands had no significant change below 200 °C, while the D- and G-bands gradually separated and the G-band showed a significant blue shift and the $FWHM_G$ exhibited a decreasing trend up to 600 °C, indicating a tending toward Raman characteristics of microcrystalline graphite.

Author Contributions: Conceptualization, M.Y.; methodology, Y.Z.; investigation, S.Z., G.J., and Y.Y.; formal analysis, S.Z.; data curation, S.Z.; writing—original draft, S.Z.; writing—review and editing, S.Z., G.J., Y.Y., H.L., F.Y., M.Y. and Y.Z.; supervision, M.Y. and Y.Z.; project administration, M.Y. and Y.Z.; funding acquisition, M.Y. and Y.Z. All authors have read and agreed to the published version of the manuscript.

Funding: This work was supported by the National Natural Science Foundation of China (Grant No. 52073072).

Institutional Review Board Statement: Not applicable.

Informed Consent Statement: Not applicable.

Data Availability Statement: Not applicable.

Conflicts of Interest: The authors declare no conflict of interest.

References

1. Robertson, J. Diamond-like amorphous carbon. *Mater. Sci. Eng. R. Rep.* **2002**, *37*, 129–281. [CrossRef]
2. Bai, L.; Zhang, G.; Lu, Z.; Wu, Z.; Wang, Y.; Wang, L.; Yan, P. Tribological mechanism of hydrogenated amorphous carbon film against pairs: A physical description. *J. Appl. Phys.* **2011**, *110*, 033521. [CrossRef]
3. Donnet, C.; Erdemir, A. Historical developments and new trends in tribological and solid lubricant coatings. *Surf. Coat. Technol.* **2004**, *180–181*, 76–84. [CrossRef]
4. Robertson, J. Properties of diamond-like carbon. *Surf. Coat. Technol.* **1992**, *50*, 185–203. [CrossRef]
5. Zhang, S.; Yan, M.; Yang, Y.; Zhang, Y.; Yan, F.; Li, H. Excellent mechanical, tribological and anti-corrosive performance of novel Ti-DLC nanocomposite thin films prepared via magnetron sputtering method. *Carbon* **2019**, *151*, 136–147. [CrossRef]
6. Al Mahmud, K.A.H.; Kalam, M.A.; Masjuki, H.H.; Mobarak, H.M.; Zulkifli, N.W.M. An updated overview of diamond-like carbon coating in tribology. *Crit. Rev. Solid State Mater. Sci.* **2014**, *40*, 90–118. [CrossRef]
7. Bewilogua, K.; Hofmann, D. History of diamond-like carbon films—From first experiments to worldwide applications. *Surf. Coat. Technol.* **2014**, *242*, 214–225. [CrossRef]
8. Grill, A. Diamond-like carbon: State of the art. *Diam. Relat. Mater.* **1999**, *8*, 428–434. [CrossRef]
9. Hauert, R. A review of modified DLC coatings for biological applications. *Diam. Relat. Mater.* **2003**, *12*, 583–589. [CrossRef]
10. Erdemir, A.; Donnet, C. Tribology of diamond-like carbon films: Recent progress and future prospects. *J. Phys. D Appl. Phys.* **2006**, *39*, R311–R327. [CrossRef]
11. Aisenberg, S.; Chabot, R. Ion-Beam Deposition of Thin Films of Diamondlike Carbon. *J. Appl. Phys.* **1971**, *42*, 2953–2958. [CrossRef]
12. Wu, W.-J.; Hon, M.-H. Thermal stability of diamond-like carbon films with added silicon. *Surf. Coat. Technol.* **1999**, *111*, 134–140. [CrossRef]
13. Cho, Y.K.; Jang, W.S.; Yoo, S.; Kim, S.G.; Kim, S.W. Synthesis of conductive Ti–C:H films on the stainless steel plates by PECVD process. *Surf. Coat. Technol.* **2008**, *202*, 5390–5394. [CrossRef]
14. Narayan, R.J. Pulsed laser deposition of functionally gradient diamondlike carbon–metal nanocomposites. *Diam. Relat. Mater.* **2005**, *14*, 1319–1330. [CrossRef]
15. Weng, K.-W.; Chen, Y.-C.; Lin, T.-N.; Wang, D.-Y. Metal-doped diamond-like carbon films synthesized by filter-arc deposition. *Thin Solid Films* **2006**, *515*, 1053–1057. [CrossRef]
16. Wu, W.-Y.; Ting, J.-M. Growth and characteristics of metal-containing diamond-like carbon using a self-assembled process. *Carbon* **2006**, *44*, 1210–1217. [CrossRef]
17. Vetter, J. 60 years of DLC coatings: Historical highlights and technical review of cathodic arc processes to synthesize various DLC types, and their evolution for industrial applications. *Surf. Coat. Technol.* **2014**, *257*, 213–240. [CrossRef]
18. Zhang, S.; Yan, F.; Yang, Y.; Yan, M.; Zhang, Y.; Guo, J.; Li, H. Effects of sputtering gas on microstructure and tribological properties of titanium nitride films. *Appl. Surf. Sci.* **2019**, *488*, 61–69. [CrossRef]
19. Souček, P.; Schmidtová, T.; Buršíková, V.; Vašina, P.; Pei, Y.T.; De Hosson, J.T.M.; Caha, O.; Peřina, V.; Mikšová, R.; Malinský, P. Tribological properties of nc-TiC/a-C:H coatings prepared by magnetron sputtering at low and high ion bombardment of the growing film. *Surf. Coat. Technol.* **2014**, *241*, 64–73. [CrossRef]
20. Zhang, S.; Xie, H.; Zeng, X.; Hing, P. Residual stress characterization of diamond-like carbon coatings by an X-ray diffraction method. *Surf. Coat. Technol.* **1999**, *122*, 219–224. [CrossRef]
21. Friedmann, T.A.; McCarty, K.F.; Barbour, J.C.; Siegal, M.P.; Dibble, D.C. Thermal stability of amorphous carbon films grown by pulsed laser deposition. *Appl. Phys. Lett.* **1996**, *68*, 1643–1645. [CrossRef]
22. Nakazawa, H.; Yamagata, Y.; Suemitsu, M.; Mashita, M. Thermal effects on structural properties of diamond-like carbon films prepared by pulsed laser deposition. *Thin Solid Films* **2004**, *467*, 98–103. [CrossRef]
23. Sheeja, D.; Tay, B.K.; Lau, S.P.; Shi, X. Tribological properties and adhesive strength of DLC coatings prepared under different substrate bias voltages. *Wear* **2001**, *249*, 433–439. [CrossRef]

24. Erdemir, A.; Donnet, C. *Tribology of Diamond and Diamond-like Carbon Films: An Overview*; Stachowiak, G.W., Ed.; Wear: Materials, Mechanisms and Practice; Wiley: London, UK, 2005; pp. 1–7. [CrossRef]
25. Li, H.; Xu, T.; Wang, C.; Chen, J.; Zhou, H.; Liu, H. Annealing effect on the structure, mechanical and tribological properties of hydrogenated diamond-like carbon films. *Thin Solid Films* **2006**, *515*, 2153–2160. [CrossRef]
26. Zhang, S.; Bui, X.L.; Li, X. Thermal stability and oxidation properties of magnetron sputtered diamond-like carbon and its nanocomposite coatings. *Diam. Relat. Mater.* **2006**, *15*, 972–976. [CrossRef]
27. Fu, R.K.Y.; Mei, Y.F.; Fu, M.Y.; Liu, X.Y.; Chu, P.K. Thermal stability of metal-doped diamond-like carbon fabricated by dual plasma deposition. *Diam. Relat. Mater.* **2005**, *14*, 1489–1493. [CrossRef]
28. Chen, X.; Peng, Z.; Fu, Z.; Wu, S.; Yue, W.; Wang, C. Microstructural, mechanical and tribological properties of tungsten-gradually doped diamond-like carbon films with functionally graded interlayers. *Surf. Coat. Technol.* **2011**, *205*, 3631–3638. [CrossRef]
29. Bai, W.Q.; Li, L.L.; Wang, X.L.; He, F.F.; Liu, D.G.; Jin, G.; Tu, J.P. Effects of Ti content on microstructure, mechanical and tribological properties of Ti-doped amorphous carbon multilayer films. *Surf. Coat. Technol.* **2015**, *266*, 70–78. [CrossRef]
30. Chiu, M.C.; Hsieh, W.P.; Ho, W.Y.; Wang, D.Y.; Shieu, F.S. Thermal stability of Cr-doped diamond-like carbon films synthesized by cathodic arc evaporation. *Thin Solid Films* **2005**, *476*, 258–263. [CrossRef]
31. Osanai, H.; Nakamura, K.; Sasaki, Y.; Koriyama, H.; Kobayashi, Y.; Enta, Y.; Suzuki, Y.; Suemitsu, M.; Nakazawa, H. Effects of annealing temperature on the mechanical, optical, and electrical properties of hydrogenated, nitrogen-doped diamond-like carbon films. *Thin Solid Films* **2022**, *745*, 139100. [CrossRef]
32. Martnez-Martnez, D.; Lpez-Carts, C.; Gago, R.; Fernndez, A.; Snchez-Lpez, J.C. Thermal Stability and Oxidation Resistance of Nanocomposite TiC/a-C Protective Coatings. *Plasma Process. Polym.* **2009**, *6*, S462–S467. [CrossRef]
33. Dillon, R.O.; Woollam, J.A.; Katkanant, V. Use of Raman scattering to investigate disorder and crystallite formation in as-deposited and annealed carbon films. *Phys. Rev. B* **1984**, *29*, 3482–3489. [CrossRef]
34. Chu, P.K.; Li, L. Characterization of amorphous and nanocrystalline carbon films. *Mater. Chem. Phys.* **2006**, *96*, 253–277. [CrossRef]
35. Tuinstra, F.; Koenig, J.L. Raman Spectrum of Graphite. *J. Chem. Phys.* **1970**, *53*, 1126–1130. [CrossRef]
36. Ferrari, A.C.; Robertson, J. Interpretation of Raman spectra of disordered and amorphous carbon. *Phys. Rev. B Condens. Matter.* **2000**, *61*, 14095–14107. [CrossRef]
37. Castiglioni, C.; Negri, F.; Rigolio, M.; Zerbi, G. Raman activation in disordered graphites of the A'_1 symmetry forbidden $k \neq 0$ phonon: The origin of the D line. *J. Chem. Phys.* **2001**, *115*, 3769–3778. [CrossRef]
38. Castiglioni, C.; Di Donato, E.; Tommasini, M.; Negri, F.; Zerbi, G. Multi-wavelength Raman response of disordered graphitic materials: Models and simulations. *Synth. Met.* **2003**, *139*, 885–888. [CrossRef]
39. Castiglioni, C.; Tommasini, M.; Zerbi, G. Raman spectroscopy of polyconjugated molecules and materials: Confinement effect in one and two dimensions. *Philos. Trans. A Math. Phys. Eng. Sci.* **2004**, *362*, 2425–2459. [CrossRef]
40. Ferrari, A.C.; Robertson, J. Raman spectroscopy of amorphous, nanostructured, diamond-like carbon, and nanodiamond. *Philos. Trans. A Math. Phys. Eng. Sci.* **2004**, *362*, 2477–2512. [CrossRef]
41. Orwa, J.O.; Andrienko, I.; Peng, J.L.; Prawer, S.; Zhang, Y.B.; Lau, S.P. Thermally induced sp^2 clustering in tetrahedral amorphous carbon (ta-C) films. *J. Appl. Phys.* **2004**, *96*, 6286–6297. [CrossRef]
42. Lin, Y.-H.; Lin, H.-D.; Liu, C.-K.; Huang, M.-W.; Chen, Y.-C.; Chen, J.-R.; Shih, H.C. Annealing effect on the structural, mechanical and electrical properties of titanium-doped diamond-like carbon films. *Thin Solid Films* **2009**, *518*, 1503–1507. [CrossRef]
43. Khamnualthong, N.; Siangchaew, K.; Limsuwan, P. Thermal Stability Evaluation of Diamond-like Carbon for Magnetic Recording Head Application using Raman Spectroscopy. *Procedia Eng.* **2012**, *32*, 888–894. [CrossRef]
44. Zhang, D.; Li, S.; Zuo, X.; Guo, P.; Ke, P.; Wang, A. Structural and mechanism study on enhanced thermal stability of hydrogenated diamond-like carbon films doped with Si/O. *Diam. Relat. Mater.* **2020**, *108*, 107923. [CrossRef]